DISEASES AND DISORDERS

IL-6–GP130 signaling protects human hepatocytes against lipid droplet accumulation in humanized liver models

Marisa Carbonaro[1], Kehui Wang[1]†, Hui Huang[1]†, Davor Frleta[1], Aditi Patel[1], Alexander Pennington[2], Mathieu Desclaux[1], Sven Moller-Tank[1], Justin Grindley[1], Judith Altarejos[1], Jun Zhong[1], Greg Polites[1], William Poueymirou[1], Stephen Jaspers[1], Christos Kyratsous[1], Brian Zambrowicz[1], Andrew Murphy[1], John C. Lin[1], Lynn E. Macdonald[1], Christopher Daly[1], Mark Sleeman[1], Gavin Thurston[1], Zhe Li[1]*

Liver steatosis is an increasing health issue with few therapeutic options, partly because of a paucity of experimental models. In humanized liver rodent models, abnormal lipid accumulation in transplanted human hepatocytes occurs spontaneously. Here, we demonstrate that this abnormality is associated with compromised interleukin-6 (IL-6)–glycoprotein 130 (GP130) signaling in human hepatocytes because of incompatibility between host rodent IL-6 and human IL-6 receptor (IL-6R) on donor hepatocytes. Restoration of hepatic IL-6–GP130 signaling, through ectopic expression of rodent IL-6R, constitutive activation of GP130 in human hepatocytes, or humanization of an *Il6* allele in recipient mice, substantially reduced hepatosteatosis. Notably, providing human Kupffer cells via hematopoietic stem cell engraftment in humanized liver mice also corrected the abnormality. Our observations suggest an important role of IL-6–GP130 pathway in regulating lipid accumulation in hepatocytes and not only provide a method to improve humanized liver models but also suggest therapeutic potential for manipulating GP130 signaling in human liver steatosis.

INTRODUCTION

Humanized liver mouse and rat models, in which donor human hepatocytes repopulate recipient rodent livers, have been widely used to study human liver biology, diseases, and therapeutics (*1*–*6*). However, it has been widely observed that engrafted human hepatocytes in both humanized liver mice and rats show defects, including increased lipid droplet accumulation (*5*–*7*). Ameliorating such defects would improve the accuracy of the models to recapitulate normal human liver biology and shed light on some of the underlying mechanisms that regulate lipid accumulation in hepatocytes. In addition, abnormal accumulation of lipid droplets in liver is a major feature of fatty liver disease, an increasing health issue in developed countries (*8*). This phenotype could provide a unique opportunity to address liver fattiness with human hepatocytes in an in vivo model.

Numerous clinical and preclinical studies suggest that cytokine imbalance plays a critical role in the pathogenesis of fatty liver disease (*9*, *10*). Interleukin-6 (IL-6) is among the major cytokines frequently observed to be dysregulated in patients with hepatic steatosis (*10*, *11*). In livers, hepatocytes receive IL-6 signals through paracrine interaction between IL-6 receptor (IL-6R) on their cell surface and IL-6 predominately produced by nonparenchymal cells, including Kupffer cells (*11*). Up to now, whether IL-6 and its downstream glycoprotein 130 (GP130) signal pathway is beneficial or detrimental in human liver steatosis remains controversial (*11*–*20*).

Here, we demonstrate that lipid droplet accumulation in humanized mouse and rat livers is associated with impaired IL-6R signaling in human hepatocytes, which is a result of incompatibility between rodent IL-6 and human IL-6R (hIL-6R) expressed on donor hepatocytes. Restoration of IL-6 pathway activity, either through ectopic expression of rodent IL-6R or through constitutive activation of GP130 in engrafted human hepatocytes, substantially reduced lipid droplet accumulation. Furthermore, supplementing human IL-6 (hIL-6) in humanized liver mice or rats not only prevented but also reversed lipid droplet accumulation in human hepatocytes. Notably, providing human myeloid cells via hematopoietic stem cell (HSC) engraftment in humanized liver mice eliminated the abnormal lipid droplets in human hepatocytes.

RESULTS

Human, but not rodent, hepatocytes engrafted in host mice or rats showed hepatosteatosis

We generated humanized liver mouse and rat models by engrafting human hepatocytes in the livers of *FSRG* (*Fah*$^{-/-}$, *Sirpa*$^{hu/hu}$, *Rag2*$^{-/-}$, *Il2rg*$^{-/-}$) mice or *FRG* (*Fah*$^{-/-}$, *Rag1/2*$^{-/-}$, *Il2rg*$^{-/-}$) rats, respectively. In both models, humanized livers showed a steatosis-like phenotype marked by positive Oil Red O staining (Fig. 1, A and B). Moreover, extensive distribution of eosin-negative vacuoles occurred in fumarylacetoacetate hydrolase (FAH)–positive areas of humanized mouse or rat livers, suggesting an accumulation of lipid droplets within human engraftments (Fig. 1, A and B). Accordingly, immunohistological analysis showed positive cytoplasmic staining of lipid binding protein 17β-hydroxysteroid dehydrogenase type 13 (HSD17B13) in all human asialoglycoprotein receptor 1 (hASGR1)–positive regions (Fig. 1, A and B), confirming

[1]Regeneron Pharmaceuticals Inc., Tarrytown, NY, USA. [2]Pyxant Labs Inc., Salt Lake City, UT, USA.
*Corresponding author. Email: zhe.li@regeneron.com
†These authors contributed equally to this work.

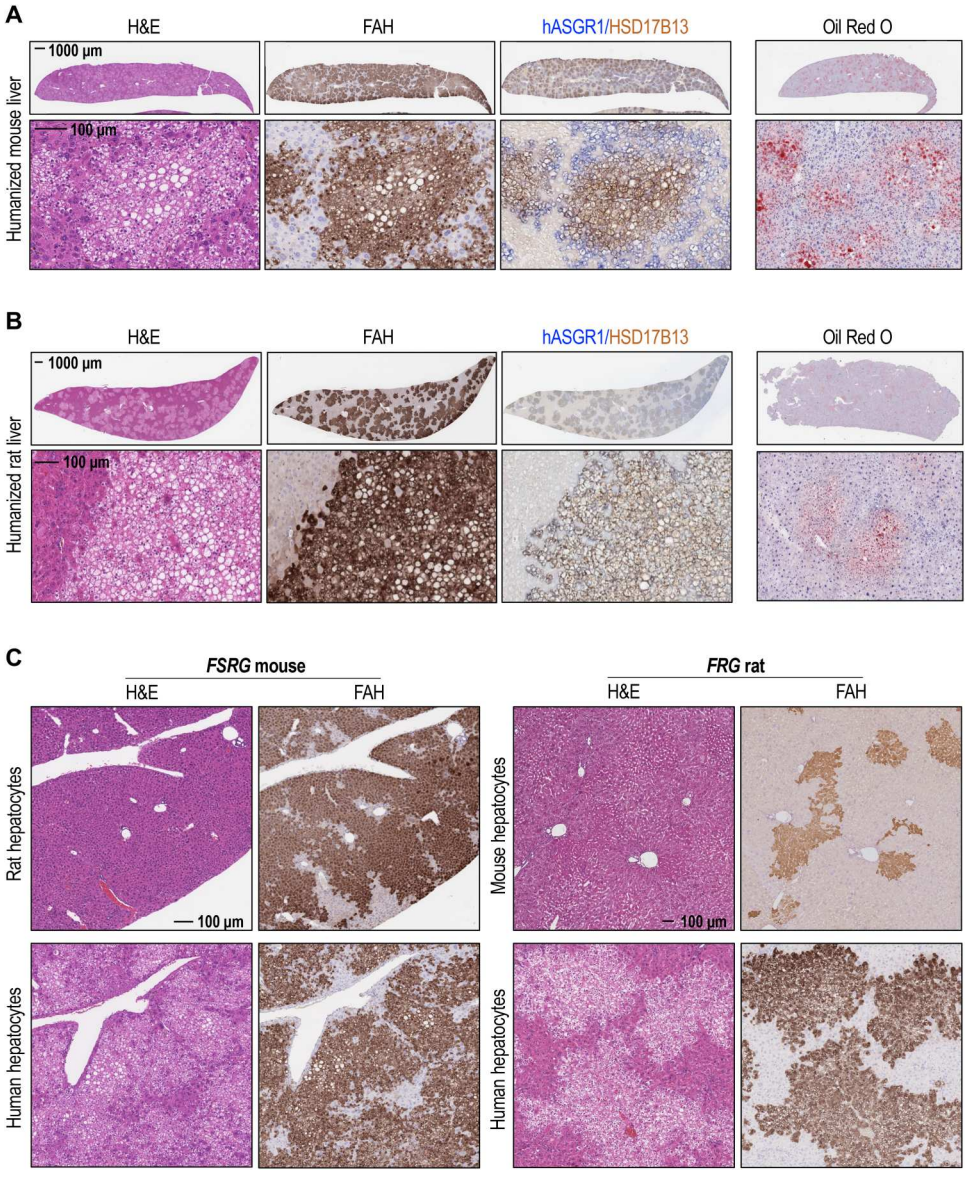

Fig. 1. Abnormal lipid accumulation in humanized liver mice and rats. (**A**) Hematoxylin and eosin (H&E) staining; FAH, hASGR1, and HSD17B13 immunohistochemistry (IHC); and Oil Red O staining of humanized mouse liver sections, collected at 12 weeks posttransplant. (**B**) H&E staining; FAH, hASGR1, and HSD17B13 IHC; and Oil Red O staining of humanized rat liver sections, collected at 7 months posttransplant. (**C**) H&E staining and FAH IHC of rat or human primary hepatocytes engrafted into *FSRG* mice (left) or mouse or human primary hepatocytes engrafted into *FRG* rat (right) livers . *FSRG* mouse livers were harvested at 13 weeks postengraftment, and *FRG* rat livers were harvested at 15 weeks posttransplant.

a human-specific hepatosteatosis phenotype in humanized liver rodents. This abnormality did not occur in rat or mouse hepatocytes engrafted in either *FSRG* mice or *FRG* rats (Fig. 1C), suggesting that it is not a result of the engraftment process. Such a phenomenon raises the possibility that lipid overaccumulation in engrafted human hepatocytes could be a result of impaired signaling in donor cells because of cross-species incompatibility between recipient rodents and human hepatocytes.

Restoration of IL-6–IL-6R signaling through ectopic expression of rodent IL-6R in human hepatocytes eliminates lipid droplet accumulation in humanized livers

Incompatibilities of ligand-receptor interactions across species have been widely observed, especially in interspecies transplantation studies [for a recent review, see (*21*)]. In the liver, a number of receptors expressed on the surface of hepatocytes needs to interact with ligands produced by other cell types to transduce downstream signals (*22*), some of which show cross-species incompatibility between murine ligands and human receptors. A lack of reactivity between murine ligands and their human receptors might contribute to the fatty phenotype in humanized liver mouse models. Such

ligand-receptor pairs include fibroblast growth factor 19 (FGF19)–FGF receptor 4 (FGFR4) (*23*), hepatocyte growth factor (HGF)–mesenchymal epithelial transition factor receptor (MET) (*24*), growth hormone (GH)–GH receptor (GHR) (*7*), oncostatin M (OSM)–OSM receptor (OSMR) (*25*), and IL-6–IL-6R (*26*). We tested this concept by overexpressing human FGF19 or by applying activating antibodies to MET receptor in humanized liver mice and found that neither restoration of FGR19-FGFR4 nor MET signaling in humanized livers lead to correction of this phenotype (fig. S1). Separately, an earlier study demonstrated that administration of human GH in humanized liver mice could correct fatty liver in humanized liver mice (*7*). However, genetic defects in the GH-GHR pathway have not been found in patients with fatty liver disease. Rather, observations both in patients and in experimental animal models show dysregulation of multiple cytokines in development of hepatic steatosis (*10*). In particular, IL-6 is among the cytokines frequently dysregulated in patients with hepatic steatosis, including nonalcoholic fatty liver disease (NAFLD) and nonalcoholic steatohepatitis (NASH) (*11*). We therefore sought to investigate the role of IL-6–IL-6R signaling in hepatic lipid droplet accumulation. As shown in Fig. 2A, treatment with mouse IL-6 (mIL-6) or rat IL-6 (rIL-6) can induce signal transducer and activator of transcription 3 (STAT3) phosphorylation in both primary murine and rat hepatocytes, but not in human hepatocytes, consistent with suboptimal interaction between mIL-6 or rIL-6 ligand and hIL-6R. We therefore hypothesized that cross-species incompatibility between mIL-6 or rIL-6 and hIL-6R might play a role in lipid droplet accumulation in humanized liver mice and rats.

To test this hypothesis, we sought to restore IL-6R signaling by ectopic expression of rodent IL-6R in humanized livers. To this end, primary human hepatocytes were transduced with lentivirus carrying *mIl6r* or *rIl6r* expression vectors before implantation into recipient mice or rats, respectively. As shown in Fig. 2B, unlike untreated cells, lentivirus-treated primary human hepatocytes responded robustly to mIL-6 treatment by elevation of STAT3 phosphorylation ex vivo. In vivo, mIL-6R expression in humanized livers was detected by in situ hybridization using a *FLAG*-specific RNAscope probe (Fig. 2C) or immunoreactivity to an antibody (fig. S2A) that recognizes a FLAG-tag sequence fused to the mIL-6R transgene. Because no selection procedure was applied before implantation, humanized livers consisted of both mIL-6R–expressing (FLAG-positive) and nonexpressing (FLAG-negative) regions of hASGR1-expressing human hepatocytes. As expected, contrary to the evident steatosis observed in FLAG-negative human hepatocytes, FLAG-positive, mIL-6R–expressing areas showed a substantial reduction, if not complete disappearance of lipid droplet accumulation (Fig. 2C and fig. S2A). Similarly, human hepatocytes expressing rIL-6R also showed efficient phospho-STAT3 (pSTAT3) activation upon rIL-6 treatment ex vivo (Fig. 2D) and lack of lipid droplet accumulation in humanized liver rats (Fig. 2E and fig. S2B). Thus, restoration of IL-6R signaling in human hepatocytes through ectopic expression of rodent IL-6R reactive to host-derived IL-6 eliminated lipid droplet accumulation in humanized livers.

Restoration of GP130 signaling through ectopic expression of constitutively active GP130 in human hepatocytes also eliminates lipid droplet accumulation in humanized livers

Upon IL-6 binding, IL-6R requires interaction with GP130 co-receptor to activate downstream pathways (*27*). Therefore, we next asked whether hepatic activation of GP130 is sufficient to prevent lipid droplet accumulation. To this end, we expressed a ligand-independent, constitutively activated form of GP130 with a deletion from Tyr^{186} to Tyr^{190} ($GP130^{Y186\text{-}Y190del}$) (*20*) in human hepatocytes through lentiviral transduction. Expression of this mutant resulted in an elevation of pSTAT3 level in primary human hepatocytes ex vivo, even without treatment with hIL-6 (Fig. 2F).

Upon engraftment of the transduced hepatocytes in recipient mouse livers, $GP130^{Y186\text{-}Y190del}$ expression was detected by in situ hybridization using an RNAscope probe specific to a *GFP* tag sequence in the transgene. As expected, humanized livers consisted of both $GP130^{Y186\text{-}Y190del}$-expressing (*GFP*-positive) and nonexpressing (*GFP*-negative) regions of hASGR1-expressing human hepatocytes (Fig. 2G). Furthermore, in humanized murine livers, contrary to the evident steatosis morphology of *GFP*-negative human hepatocytes, *GFP*-positive, $GP130^{Y186\text{-}Y190del}$-expressing areas showed a complete absence of lipid droplet accumulation (Fig. 2G). Therefore, GP130 activation is sufficient to protect humanized engraftments from hepatosteatosis in humanized liver mice.

hIL-6 prevents lipid droplet accumulation in human hepatocytes

Our observations on correction of liver fattiness through restoration of hepatic IL-6–GP130 signaling suggested that supplementation with hIL-6 in host animals would protect humanized livers from hepatic steatosis. To test this hypothesis, immediately before human hepatocyte implantation, *FSRG* mice were dosed with adeno-associated virus 9 (AAV9) encoding an expression vector in which the *hIL6* coding region was placed under control of the muscle-specific promoter, *MHCK7*, a hybrid promoter with the enhancer/promoter regions of mouse muscle creatine kinase (*Ck*) and α-myosin heavy chain genes. As a result, hIL-6 expression was maintained in the serum of humanized liver mice until 8 weeks postimplantation, when tissues were harvested. At 8 weeks postimplantation of human hepatocytes, AAV9-*hIL6*–dosed *FSRG* mice expressed 1.7 to 4.8 ng/ml of hIL-6 in the serum and exhibited robust phosphorylation of STAT3 in the liver (Fig. 3A). In contrast, neither serum hIL-6 nor liver STAT3 phosphorylation were detectable in control humanized liver mice. In addition, we also observed increased expression of IL-6 target genes, including human *SOCS3* and *SAA2*, in the livers (fig. S3). Notably, compared to control animals with similar amounts of human engraftment, humanized livers of mice expressing hIL-6 showed a substantial decrease of the eosin-negative area (two- to sixfold, almost to baseline level), mostly in FAH^+ regions, indicative of a reduction of lipid droplet accumulation (Fig. 3B) and supporting a protective role of hIL-6 against hepatic steatosis in this model.

Systemic supplementation of hIL-6 through AAV dosing resulted in serum levels of the cytokine that are higher than the normal range, which could cause nonphysiological and potentially detrimental effects. To address these concerns, we generated a recipient mouse with an *FSRG* background in which the coding region of murine *Il6* allele was replaced with its human homolog. In such an animal, human *IL6* gene expression is controlled by the endogenous murine *Il6* promoter. Lipopolysaccharide (LPS) treatment resulted in induction of hIL-6 expression in the serum of mice with homozygous humanized *Il6* allele (Fig. 4A). In comparison, only murine IL-6 was detected in mice with wild-type murine *Il6*

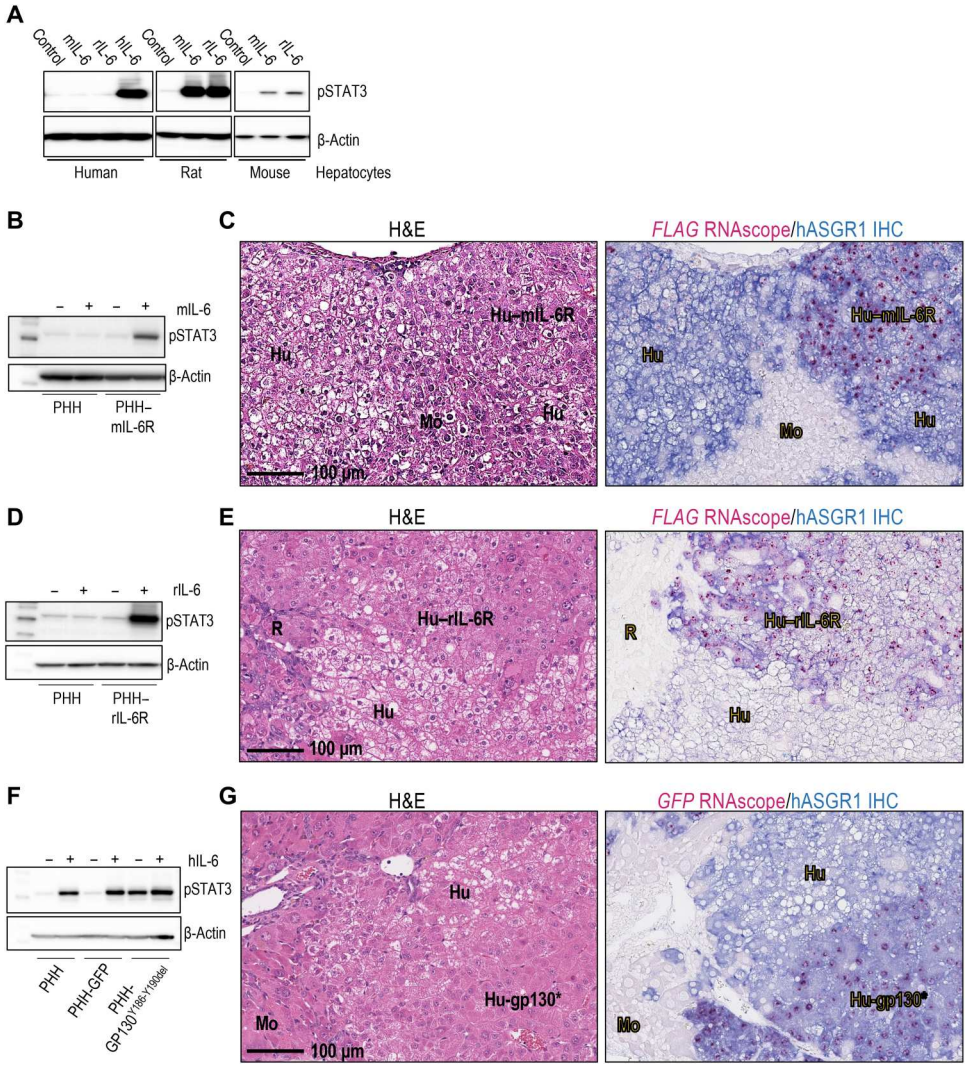

Fig. 2. Ectopic overexpression of rodent IL-6R or constitutively active GP130 protects human hepatocytes from lipid droplet accumulation in humanized liver models. (**A**) Phospho-STAT3 (pSTAT3) Western blot of primary human, rat, or mouse hepatocytes treated with hIL-6, rIL-6, or mIL-6. (**B**) pSTAT3 Western blot of protein lysates from nontransduced primary human hepatocytes (PHH) or PHH transduced with lentivirus carrying *mIl6r* and treated with mIL-6. (**C**) H&E and hASGR1-IHC/*FLAG*-RNAscope double staining of *FSRG* mouse liver sections with engrafted PHH expressing mIL-6R. Livers were harvested 14 weeks postengraftment. mIL-6R–expressing human hepatocytes (Hu–mIL-6R) were detected using a human-specific ASGR1 antibody (blue) and *FLAG* RNAscope probe (pink). Nontransduced human hepatocytes (Hu) were positive for hASGR1, but not *FLAG*. Nonengrafted regions (Mo) are negative for both hASGR1 and *FLAG* RNAscope. Experiment was performed twice with two different hepatocyte donors, $n = 6$ per cohort. (**D**) pSTAT3 Western blot of nontransduced PHH or PHH transduced with lentivirus carrying rat *Il6r* and treated with rIL-6. (**E**) H&E and hASGR1-IHC/*FLAG*-RNAscope staining of *FRG* rat liver sections with engrafted PHH expressing rIL-6R. Livers were harvested 22 weeks postengraftment. rIL-6R–expressing human hepatocytes (Hu–rIL-6R) were positive for both hASGR1 and *FLAG*. Nontransduced human hepatocytes (Hu) were hASGR1-positive, but *FLAG*-negative. Nonengrafted regions (R) are negative for both hASGR1 and *FLAG*. The experiment was performed twice, $n = 5$ per cohort. (**F**) pSTAT3 Western blot of protein lysates from nontransduced PHH or PHH transduced with lentivirus carrying *GFP* (control) or $GP130^{Y186\text{-}Y190del}$. (**G**) H&E and hASGR1-IHC/*GFP*-RNAscope double staining of *FSRG* mouse liver sections with engrafted PHH expressing $GP130^{Y186\text{-}Y190del}$ (Hu-GP130*). Livers were harvested 8 weeks postengraftment. Hu-GP130* hepatocytes were detected by hASGR1 IHC and *GFP* RNAscope. Nontransduced human hepatocytes (Hu) were positive for hASGR1, but not *GFP*. Nonengrafted regions (Mo) are negative for both. The experiment was performed twice with two hepatocyte donors, $n = 3$ per cohort.

alleles (Fig. 4A). In heterozygous mice, in which the *Il6* locus has one allele each of human and murine *IL6* genes, both human and murine IL-6 proteins were detected in the serum (Fig. 4A). After liver humanization, human C-reactive protein (hCRP) was detected in the serum of both $FSRG\text{-}Il6^{HumIn(het)}$ and $FSRG\text{-}Il6^{HumIn(homo)}$ mice, but not $FSRG\text{-}Il6^{WT}$ mice (fig. S4A), confirming a human-specific IL-6 response in humanized liver mice with humanized *Il6* allele. Consistently, human hepatocytes engrafted in the livers of $FSRG\text{-}Il6^{WT}$ mice showed abundant lipid droplet accumulation, whereas humanized livers in both $FSRG\text{-}Il6^{HumIn(het)}$ or $FSRG\text{-}Il6^{HumIn(homo)}$ mice showed significant alleviation of the fatty phenotype, with two- to threefold reduction of the eosin-negative vacuole area in FAH^{+} regions (Fig. 4B), demonstrating a role of endogenous hIL-6 in protecting human hepatocytes from lipid droplet accumulation in this model.

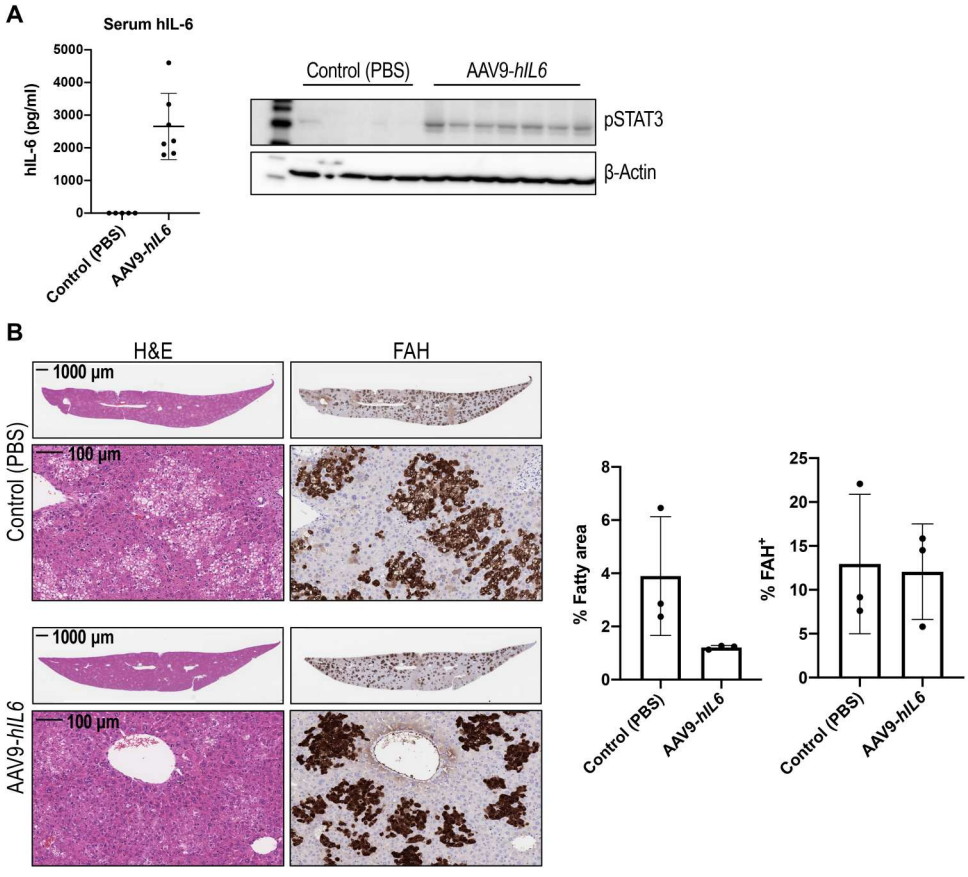

Fig. 3. Systemic supplementation with hIL-6 prevents lipid droplet accumulation in humanized livers. (**A**) hIL-6 enzyme-linked immunosorbent assay (ELISA) of serum and pSTAT3 Western blot of liver protein extract of PHH-engrafted mice treated with AAV9-*hIL6* ($n = 7$) versus phosphate-buffered saline (PBS) control ($n = 5$) at the time of hepatocyte transplant. (**B**) H&E and FAH IHC of mouse livers 8 weeks after AAV9-*hIL6* dosing and PHH transplant. Quantification of the percentage of fatty area and percentage of FAH positivity confirms a decrease in lipid accumulation in hIL-6–treated mice despite similar humanization levels. Data are shown as means ± SD (each dot represents one mouse; two to three liver lobes per mouse were analyzed).

hIL-6 reverses lipid droplet accumulation in human hepatocytes

Next, we asked whether hIL-6 treatment can reverse the steatosis phenotype in humanized livers. This question was addressed in both humanized liver mouse and rat models. Rather than administering AAV9-*hIL6* before hepatocyte implantation, viral dosing was performed in *FSRG* mice and *FRG* rats that were already engrafted with human hepatocytes. At 4 weeks after AAV9-*hIL6* dosing, tissues were collected. Again, hIL-6 expression and hepatic IL-6 pathway activation was confirmed by serum hIL-6 and hCRP, liver pSTAT3, and quantitative reverse transcription polymerase chain reaction (qRT-PCR) for IL-6 target genes (figs. S5 and S6). In both mouse (Fig. 5A) and rat (Fig. 5B) models, hIL-6 dosing led to a nearly complete elimination of lipid droplet accumulation, marked by robust reduction of eosin-negative vacuoles in FAH^+ regions and disappearance of Oil Red O staining in humanized livers. Thus, activated IL-6R signaling in human hepatocytes not only prevents but also reverses hepatic steatosis formation in humanized liver rodents. In addition, dosing with human OSM (hOSM), another hepatic GP130/STAT3 pathway activating ligand also led to correction of liver fattiness in humanized liver mice (fig. S7), supporting a protective role of GP130 pathway against lipid droplet accumulation in human hepatocytes.

IL-6–producing human Kupffer cells protect human hepatocytes from lipid droplet accumulation in humanized liver mice

Kupffer cells have long been known to be one of the major sources of IL-6 in the liver (*28*, *29*). These cells are located adjacent to hepatocytes where Kupffer cell–derived IL-6 could support IL-6R pathway activation in nearby hepatocytes without elevating circulating IL-6 to harmful levels. We therefore attempted to address the role of Kupffer cells in protecting human hepatocytes from lipid droplet accumulation by reconstituting human immune cells in *FSRG* mice before human hepatocyte implantation (Fig. 6A). Human fetal liver (FL) cells containing hematopoietic stem cells (HSCs) were engrafted into irradiated neonatal *FSRG* pups. By week 12, about 25 to 50% of total leukocytes in the peripheral blood of these mice were human immune cells expressing human CD45 (hCD45) (fig. S8A). Impressively, abundant *hCD68*-positive cells that also express human *IL6* were detected in the livers of these animals, suggesting the engraftment of human Kupffer cells (Fig. 6B). Following human immune cell reconstitution, human

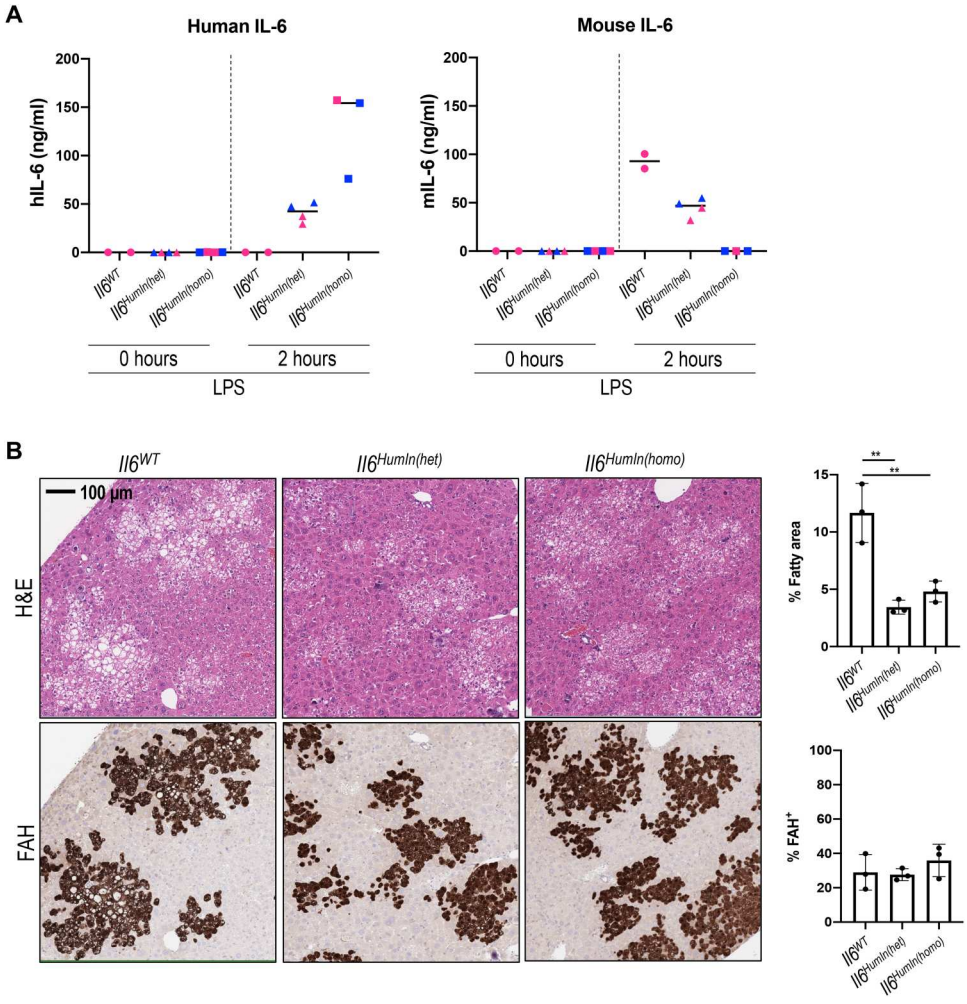

Fig. 4. Humanization of the *Il6* gene in recipient mice results in hIL-6 expression in Kupffer cells and correction of fatty phenotype of humanized livers. (**A**) hIL-6 or mIL-6 levels detected in the plasma of *FSRG-Il6*^{WT}, *FSRG-Il6*$^{HumIn(het)}$, or *FSRG-Il6*$^{HumIn(homo)}$ mice either before or after LPS treatment for 2 hours (1 mg/kg, intraperitoneal injection). Blue and pink icons represent male and female mice, respectively. (**B**) H&E staining and FAH IHC of liver sections of PHH-engrafted *FSRG-Il6*^{WT}, *FSRG-Il6*$^{HumIn(het)}$, or *FSRG-Il6*$^{HumIn(homo)}$ mice, 7 weeks after engraftment. Quantification shows the percentage of fatty area (negative H&E staining) and percentage of FAH$^+$ staining [means ± SD; three liver sections per group; $^{**}P < 0.01$ one-way analysis of variance (ANOVA)].

hepatocytes were then implanted to repopulate the liver parenchyma to generate double-humanized mice engrafted with both human immune system (HIS) and human hepatocytes (HuHEP) (Fig. 6A). As shown in Fig. 6C, hCD45-positive human immune cells intermingled with FAH$^+$ human hepatocytes in the livers of double-humanized mice. Most of the hCD45-positive cells in the liver were also hCD68 positive (fig. S8B). We confirmed the expression of hIL-6 in the serum of these mice at physiological levels, as well as expression of hCRP produced by engrafted human hepatocytes, suggesting that the IL-6 signaling pathway was restored in the double-humanized mice (fig. S8A). Notably, in contrast to the evident hepatic steatosis in humanized liver mice without human immune cells (Fig. 6C, top), humanized livers engrafted with human immune cells showed very low, if any, lipid droplet accumulation (Fig. 6C, bottom), indicating a role of engrafted human Kupffer cells in protection of human hepatocytes from steatosis.

To validate the role of engrafted human Kupffer cells, we pharmacologically depleted this cell population in the livers of double-humanized mice and assessed whether such treatment would lead to lipid droplet accumulation in human hepatocytes. The colony-stimulating factor 1 receptor (CSF1R) pathway has been shown to serve as a critical survival signal for macrophages including Kupffer cells (*30*). In our study, we specifically depleted human Kupffer cells by blocking the interaction between hCSF1R, but not mCSF1R, and its ligands with a human-specific CSF1R antibody. As shown in Fig. 6D, hCD68-expressing cells in humanized livers of HIS-HuHEP mice were almost completely depleted upon hCSF1R antibody treatment. However, expression of other nonmacrophage human immune cell markers such as *hCD3* and *hCD20* showed only moderate changes (fig. S8D), implying that the anti-hCSF1R antibody specifically ablated hCD68-positive cells in livers of HIS-HuHEP mice. Impressively, RNA expression of human *IL6* and its target genes *hSOCS3*, *hSAA2*, and *hCRP* in the liver, as well as hCRP protein in the serum, was markedly decreased (fig. S8, C and D), and extensive steatosis reoccurred in anti-hCSF1R antibody–treated HIS-HuHEP mice (Fig. 6E). Immunohistochemical analysis

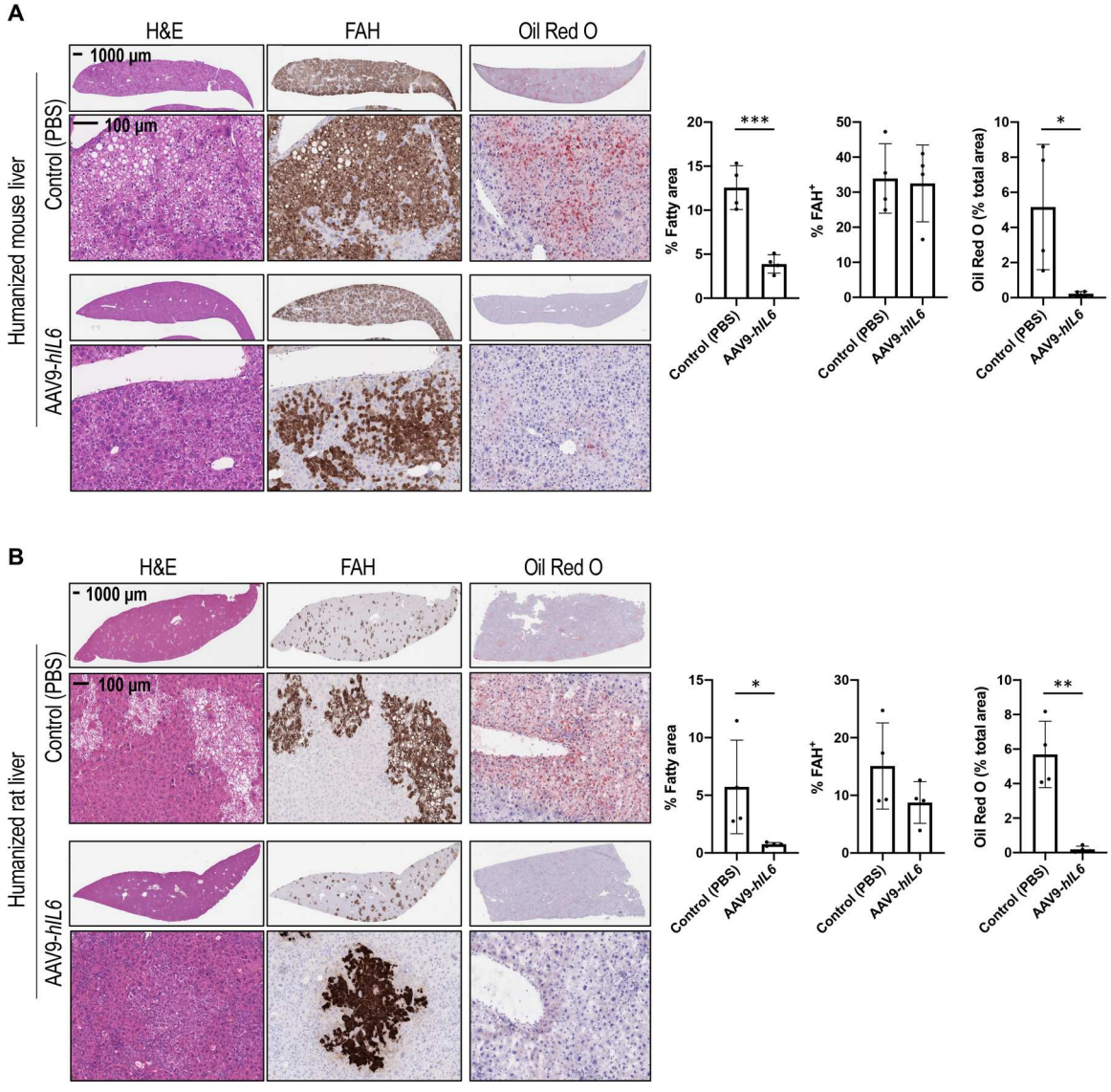

Fig. 5. hIL-6 overexpression corrects lipid droplet accumulation in humanized liver mice and rats. (**A**) H&E staining, FAH IHC, and Oil Red O staining of liver sections from humanized liver mice treated with AAV9-*hIL6* or PBS control 8 weeks after PHH transplantation and collected 4 weeks after AAV dosing. The experiment was performed three times, with two different hepatocyte donors. Quantification of the percentage of fatty area (negative H&E staining), FAH, and Oil Red O staining shows means ± SD from one experimental repeat. Each dot represents one mouse ($n = 4$ per group); two to three liver lobes per mouse were analyzed. (**B**) H&E staining, FAH IHC, and Oil Red O staining on liver sections from humanized liver rats treated with AAV9-*hIL6* versus PBS at 12 weeks post-PHH transplant and collected 4 weeks after AAV dosing ($n = 4$ per group). Quantification of the percentage of fatty area (negative H&E staining), FAH, and Oil Red O staining shows means ± SD (each dot represents one rat; two to three liver lobes per rat were analyzed). *$P < 0.05$, **$P < 0.01$, and ***$P < 0.001$; unpaired *t* test.

confirmed a more than threefold increase in lipid droplet accumulation, marked by eosin-negative vacuoles in FAH$^+$, humanized regions of the livers (Fig. 6E). Therefore, Kupffer cells producing hIL-6 play a major role in controlling lipid droplet accumulation in hepatocytes in this model.

DISCUSSION

Hepatic steatosis in humanized liver rodent models, resulting from incompatibility between human hepatocyte–expressed receptors and host-derived ligands, provides an opportunity to identify important signaling pathways involved in fatty liver disease. Here, we addressed the role of IL-6–IL-6R/GP130 signaling in human hepatosteatosis. First, we demonstrated that excessive lipid droplet accumulation in humanized livers is associated with incompatibility between rodent IL-6 ligand expressed by nonparenchymal cells of host animals and hIL-6R expressed on donor hepatocytes. We showed that lipid accumulation could be corrected by ectopic expression of rodent IL-6R or constitutive activation of GP130 in donor hepatocytes. Furthermore, supplementation of hIL-6 systemically, either via ectopic expression or genetic humanization of the murine *Il6* allele, again corrected the hepatosteatosis. Last, engraftment of human Kupffer cells into host animals also corrected the fatty phenotype. Our results in humanized rodent liver models

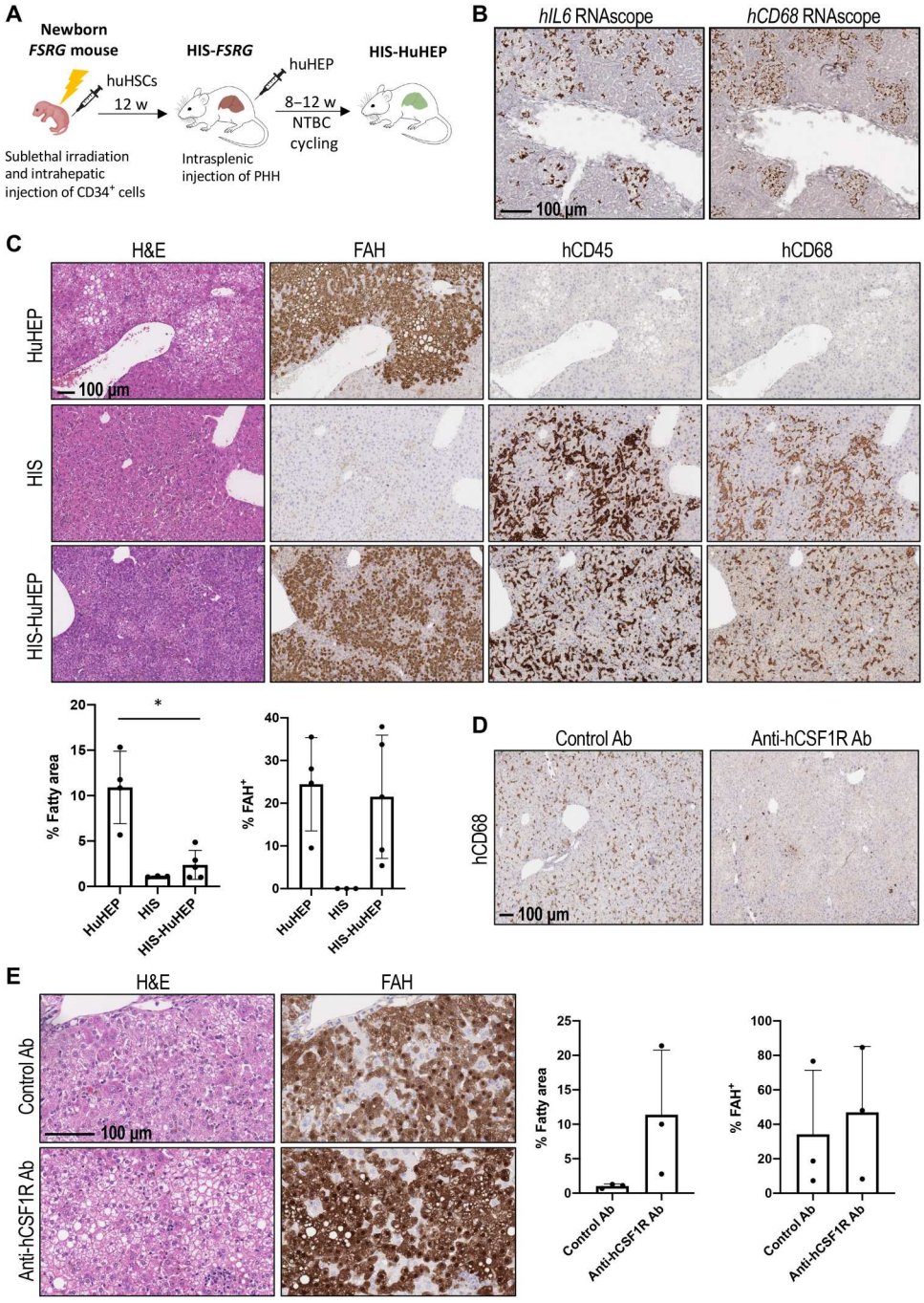

Fig. 6. Human Kupffer cell engraftment in humanized liver mice leads to correction of fatty phenotype in human hepatocytes. (**A**) Scheme of dual engraftment of human immune system (HIS) and human hepatocytes (HuHEP). huHSCs, human HSCs; NTBC, 2-(2-nitro-4-trifluoromethylbenzoyl)-1,3-cyclohexanedione. (**B**) *hIL6* and *hCD68* RNAscope staining of adjacent liver sections of HIS-engrafted *FSRG* mice after 2 hours of LPS treatment (1 mg/kg, intraperitoneal injection). (**C**) H&E and FAH, hCD45, and hCD68 IHC staining of liver sections of mice engrafted with HuHEP only (HuHEP), HIS only (HIS), or dual-engrafted HIS-HuHEP. Quantification shows a correction of fatty liver phenotype in HIS-HuHEP versus HuHEP mice (each dot represents one mouse; two to three liver lobes per mouse were analyzed; $*P < 0.05$, one-way ANOVA). (**D**) hCD68 IHC of liver sections from double-humanized HIS-HuHEP mice treated with either control antibody (control Ab) or an anti-hCSF1R antibody (anti-hCSF1R Ab) (20 mg/kg, two times per week), starting at the time of PHH transplant. The experiment was performed three times, with three different HSC donors. (**E**) H&E staining and FAH IHC of liver sections from control Ab or anti-hCSF1R Ab–treated HIS-HuHEP mice. Quantification shows means ± SD from one experimental repeat with a single HSC donor (each dot represents one mouse; two to three liver lobes per mouse were analyzed; $*P < 0.05$, one-way ANOVA).

reveal a role for hepatic GP130 signaling, maintained by IL-6 that is normally provided by nonparenchymal liver cells, in protecting hepatocytes from excessive lipid accumulation.

Here, we used multiple approaches to demonstrate the importance of the hepatic IL-6–GP130 signaling pathway in regulating liver fattiness. Each approach has its own advantage and limitations. For example, consistent observations in both *FSRG* mouse and *FRG* rat models strengthened the rationale of the cross-species incompatibility hypothesis as the mechanism of hepatosteatosis phenotypes in humanized liver animals. However, only *FSRG* mice were used in the human Kupffer cell engraftment and *Il6* allele humanization experiments because of technical challenges of humanizing *Sirpa* and *Il6* alleles in *FRG* rats. In addition, systemic overexpression of hIL-6 by AAV dosing results in serum concentrations of the ligand much higher than physiological levels and could produce nonphysiologic effects. This limitation was addressed by either genetically humanizing the *Il6* allele in host mice or engrafting IL-6–expressing human Kupffer cells through HSC implantation. In *FSRG-Il6*^{HumIn} mice, hIL-6 expression is controlled by the promoter of the host animal and regulated physiologically, thus resulting in normal levels of IL-6. However, genes encoding other paracrine factors including potential GP130 activating cytokines were not humanized, potentially masking roles for other ligands. Therefore, it is not unexpected that steatosis in humanized livers in *FSRG-Il6*^{HumIn} mice was reduced but not completely eliminated. Two examples of such factors are GH and OSM. Similar to IL-6, both mGH and mOSM show species specificities in receptor binding (*7*, *25*), and hepatosteatosis in humanized liver mice can be corrected by supplementing with high levels of either hGH (*7*) or hOSM. Humanization of these two genes in *FSRG-Il6*^{HumIn} host mice might result in further amelioration of hepatosteatosis in humanized livers. In liver humanization models, Kupffer cell–derived hIL-6 appears to be sufficient to correct steatosis in human hepatocytes, as depletion of engrafted human Kupffer cell through anti-hCSF1R monoclonal antibody treatment reproduced the fatty liver phenotype. However, in normal liver, some sinusoidal endothelial cells also express IL-6 in addition to Kupffer cells (*31*). Such a source, which is present in the genetically humanized *Il6* model but not in the double-humanized HIS-HuHEP model, could provide hIL-6 and maintain hepatic GP130 signaling upon Kupffer cell depletion. Previous studies have shown that removal of hepatic macrophages did not induce hepatosteatosis in mouse models (*32*–*34*). In contrast, Kupffer cell depletion showed a preventive effect on high-fat diet-induced pathological changes, including hyperlipidemia, in mouse livers (*33*, *34*). These observations suggest that Kupffer cells might be dispensable in preventing liver fattiness in the presence of other IL-6–producing cells. Notably, although hepatocytes have been shown to express IL-6 protein under certain conditions (*35*), no evidence of hepatic parenchymal IL-6 expression was observed in our humanized liver animals.

Our study demonstrated a critical role of IL-6–IL-6R cis-signaling in controlling steatosis in humanized livers. However, we cannot rule out the involvement of IL-6/soluble IL-6R trans-signaling through GP130. Because human GP130 shows no species preference in binding to IL-6/soluble IL-6R complex (*36*), mIL-6/soluble mIL-6R complex might activate GP130 pathway in humanized livers even without hIL-6, albeit not strong enough to correct steatosis. The impact of IL-6/soluble IL-6R trans-signaling could be tested by treatment of humanized liver mice with soluble GP130Fc, which blocks IL-6 trans- but not cis-signaling and assesses the degree of fatty liver phenotype exacerbation.

Although an ameliorating effect of IL-6R/GP130 signaling in fatty liver disease was demonstrated in this report, elevated IL-6 levels are frequently detected in patients with fatty liver and have been suggested as a contributing factor in progression of the disease (*9*–*11*, *13*, *37*). Thus, potential feedback mechanisms might exist among pathogenesis of liver fattiness, IL-6 ligand production, and hepatic IL-6R–GP130 pathway regulation. Further study to unveil such regulatory networks is warranted.

Defects in IL-6–GP130 signaling appear to contribute to hepatic steatosis in humanized liver models. However, increased liver fat has not been reported as a side effect in therapeutic settings of IL-6R blockade [for a review, see (*38*)]. One potential explanation is that other GP130-STAT3 activating ligands could compensate for diminished IL-6 pathway activity and, thus, protect hepatocytes from lipid accumulation. Besides IL-6, a number of hepatic GP130 activating cytokines have been identified, such as OSM, IL-11, etc. (*27*). In addition, leptin receptor is similar to GP130 in that it also activates STAT3 upon binding to its ligand, leptin (*39*). A recent clinical study demonstrated that administration of modified leptin reduced hepatic fat in patients with NAFLD (*40*). Therefore, administration of other GP130 and/or STAT3 activating ligands or reagents might be beneficial in fatty liver disease, with fewer potential pleiotropic effects than IL-6.

Lipid droplet accumulation in humanized liver models represents a major defect that greatly compromises the ability to model human liver biology and disease. Our observations show an important role of both Kupffer cell–derived IL-6 and its downstream IL-6R/GP130 signaling in regulating lipid accumulation in hepatocytes. These findings not only provide a method to improve humanized liver animal models but also suggest therapeutic potential for manipulating GP130 signaling in human liver steatosis.

MATERIALS AND METHODS

Animals

FSRG and *FSRG-Il6*^{HumIn} mice were generated with VelociGene and VelociMouse technologies as described previously (*41*, *42*). *FRG* rats were generated as previously described (*6*). All studies were done in accordance with the Institutional Animal Care and Use Committee guidelines at Regeneron Pharmaceuticals Inc. Animals were maintained with drinking water containing 2-(2-nitro-4-trifluoromethylbenzoyl)-1,3-cyclohexanedione (NTBC) at a concentration of 8 or 16 mg/liter for mice or rats, respectively. NTBC was purchased from Medinoah (90-1596). The drinking water also contained antibiotics, sulfamethoxazole (640 μg/ml; RPI S47000) and trimethoprim (128 μg/ml; RPI T59000), in 3% dextrose water. For diet, mice received the PicoLab High Energy Mouse Diet (5LJ5) and rats received the PicoLab Rodent Diet 20 (5053).

Hepatocyte transplantation

Cyro-preserved rat (Sprague-Dawley; male) and mouse (C57Bl/6) hepatocytes were purchased from Thermo Fisher Scientific (RTCP10) and Yecuris (20-0019), respectively. Human cyroplatable primary hepatocytes were purchased from BioIVT (female, F00995-P and male, M00995-P). An adenoviral vector expressing human urokinase (uPA) was purchased from Yecuris (CuRx uPA Liver Tx Enhancer, 20-0029) and was given by tail vein intravenous

injection at 1.25×10^9 PFU (plaque-forming units) per 25 g of body weight in 100-μl sterile phosphate-buffered saline (PBS), 24 hours before hepatocyte transplant. Hepatocyte number and viability was determined using a ViaStain AOPI staining solution (Nexcelom, CS2-0106), using the Nexcelom Cellometer Auto 2000. Mouse and rat transplantations were performed as described previously (*3*, *6*). In general, transplantations were done in female *FSRG* mice or mix-gendered *FSRG-Il6*^{HumIn} mice at ages of 6 to 9 weeks or male *FRG* rats at ages of about 9 to 12 weeks.

HSC engraftment and immune check

Human FL samples were obtained from Advanced Bioscience Resources (Alameda, CA) with proper consent. Single-cell suspension of human FL tissue was prepared by collagenase D digestion (100 ng/ml; Roche) for 25 min at 37°C. hCD34$^+$ HSCs were isolated from the cell suspension by positive immunomagnetic selection using anti-hCD34 microbeads according to the manufacturer's instructions (Miltenyi Biotec). Mixed-gendered newborn pups were sublethally irradiated (360 cGy; X-RAD 320 irradiator) 4 to 24 hours before an intrahepatic injection of 1×10^5 human FL-derived CD34$^+$ cells. Engraftment with HIS was checked by retro-orbital bleed of mice 12 weeks post-HSC injection, and red blood cell–lysed blood cells were analyzed by fluorescence-activated cell sorting for hCD45 (Thermo Fisher Scientific, #MHCD4518; clone HI30) and mouse CD45 (BD Biosciences, #557659; clone 30-F11, RRID:AB_396774). Upon engraftment check, mice were subjected to human hepatocyte transplantation.

Enzyme-linked immunosorbent assays

Blood was collected from the submandibular vein and spun in MiniCollect serum separator tubes (#450472). Engraftment of human hepatocytes was monitored using the human albumin enzyme-linked immunosorbent assay (ELISA) kit (abcam, ab108788). hIL-6, mIL-6, and hCRP were measured using SimpleStep ELISA kits (abcam, ab178013, ab222503, and ab260058, respectively). FGF19 was detected using the human FGF19 ELISA kit (abcam, ab230943).

Hepatocyte culture and Western blotting

Primary human, mouse, or rat hepatocytes were thawed in cryopreserved hepatocyte recovery medium (CM7000, Thermo Fisher Scientific) and plated in Williams E Media, with no phenol red (A1217601, Thermo Fisher Scientific) with primary hepatocyte thawing/plating supplements (CM3000, Thermo Fisher Scientific). Twenty-four hours postplating, the medium is changed and primary hepatocyte maintenance supplements (CM4000, Thermo Fisher Scientific) and 1% fetal bovine serum (FBS) are added. Hepatocytes were treated with recombinant hIL-6 (ab119444), mIL-6 (ab238300), rIL-6 (Cell Applications, RP3009), human HGF (R&D Systems, 294-HG-025), or mouse HGF (R&D Systems, 2207-HG-025) for 15 min at 50 ng/ml. Cells were lysed using radioimmunoprecipitation assay buffer (Thermo Fisher Scientific, 89900), containing protease and phosphatase inhibitors (Thermo Fisher Scientific, A32965 and 88667), run by SDS–polyacrylamide gel electrophoresis and probed using antibodies against pSTAT3 (Cell Signaling Technology, 9145, RRID:AB_2491009), total STAT3 (Cell Signaling Technology, 4904, RRID:AB_331269), pMET (Cell Signaling Technology, 3077, RRID:AB_2143884), and β-actin (Sigma-Aldrich, A5316, RRID:AB_476743).

Histology, immunohistochemistry, and RNAscope

Livers were fixed in 10% normal buffered formalin for 24 hours, washed, and stored in 70% ethanol until paraffin embedding and sectioning. Sections were stained by hematoxylin and eosin (H&E), according to standard protocols (staining performed by Histoserv Inc.). Engrafted hepatocytes were detected by immunohistochemistry (IHC) staining for FAH (abcam, ab151998) and human ASGR1 (abcam, ab254261), HSD17B13 (Sigma-Aldrich, HPA029125; RRID:AB_10601580), and FLAG (abcam, ab205606; RRID:AB_2916341), and human immune cells were detected using antibodies against hCD45 (Agilent, GA75161-2; RRID:AB_2661839) and hCD68 (Agilent, GA60961-2; RRID:AB_2661840). RNAscope probes for *hIL6* (310371), *mIl6* (315891), *hCD68* (818681), *mCd68* (316611), *GFP* (400281), and *FLAG* (1139121-S1) were purchased from Advanced Cell Diagnostics. Oil Red O staining was performed on livers fresh-frozen in Tissue-Tek O.C.T. Compound (Thermo Fisher Scientific, 14-373-65). All histology slides were scanned using a Leica Aperio AT2 scanner. FAH IHC, H&E, and Oil Red O staining were quantified using ImageJ. Statistical analysis was performed using Prism 8 by GraphPad.

AAV production and delivery

AAV production and delivery was performed as previously described with slight modifications (*6*). Recombinant AAV was produced by transient transfection of human embryonic kidney (HEK) 293T cells. Briefly, cells were transfected with AAV Rep-Cap, Adenovirus Helper, and AAV genome plasmids using PEI-Max (Polysciences). Virus-containing supernatants were concentrated by tangential flow filtration, and cells were lysed by sequential freeze and thaw (three times). Lysates were treated with benzonase (Millipore Sigma) for 1 hour at 37°C and clarified by centrifugation and filtration (0.2 μm of polyether sulfone (PES)). AAV was purified from clarified cell lysates and concentrated supernatant by iodixanol gradient ultracentrifugation. Virus fractions were concentrated and buffer-exchanged to 1× PBS + 0.001% Pluronic F68 (Thermo Fisher Scientific) using Amicon 100 kDa MWCO Ultra Centrifugal filters (Millipore Sigma). AAV genomes were quantified by qPCR using TaqMan primers and probes specific for inverted terminal repeats. A standard curve was generated using serial dilutions of virus with a known concentration. AAVs were delivered intravenously by tail vein injection at 5×10^{11} viral genomes (VG) per mouse. Animals were randomized before AAV injection based on serum human albumin levels.

Lentiviral vector production, titration, and infection

Lentiviral vector production, titration, and infection were performed as previously described with slight modifications (*6*). Lentiviral particles were produced following standard Lipofectamine-mediated cotransfection of HEK 293 T cells with the transfer plasmid encoding *mIl6r*, *rIl6r*, or human *GP130*$^{Y186\text{-}Y190del}$ under the cytomegalovirus (CMV) promoter (*pLVX-CMV-*, subcloned from *pLVX-EF1a-IRES-puro* plasmid, Takara), a second-generation packaging plasmid encoding the *gag*, *pol*, and *rev* genes (*psPAX2*, obtained from the Tronolab at Ecole Polytechnique Fédérale de Lausanne, Switzerland) and a plasmid encoding the vesicular stomatitis virus envelope glycoprotein G (VSV-G) as an envelope plasmid (*pMD2-G*, Tronolab). The day before transfection, cells were washed with PBS solution and detached from the vessel with

TrypLE Express (Life Technologies). After neutralization of TrypLE Express with cell medium containing FBS, cells were centrifuged at 1200 rpm for 5 min at 25°C, then resuspended in complete Dulbecco's modified Eagle's medium, counted, and seeded in 150-mm cell culture dishes at a density of 10×10^6 cells per plate. On the day of transfection, the cell culture medium was replaced by fresh Opti-MEM medium (Gibco/Life Technologies) and supplemented with 25 nM chloroquine (Sigma-Aldrich). The DNA mix was prepared by mixing 20 μg of transfer plasmid DNA, 20 μg of packaging plasmid, and 10 μg of envelope plasmid, as well as 1.5 ml of Opti-MEM with 60 μl of PLUS Reagent (Life Technologies). In parallel, 100 ml of Lipofectamine TLX (Life Technologies) was diluted in 1.5 ml of Opti-MEM medium. DNA mix was then added to the Lipofectamine mix, and the new combined solution was incubated at room temperature for 20 min before being added directly to the cells dropwise. The culture medium was changed 6 to 8 hours after transfection, and the cells were then incubated for 48 hours at 37°C in an incubator with 5% CO_2 atmosphere. At day 2 post-transfection, cell media containing the lentiviral particles were centrifuged for 10 min at 3000 rpm to remove the debris and then passed through a 0.45-μm pore size filter. The filtered supernatants were then treated with deoxyribonuclease (DNAse) (1 μg/ml) and 1 mM $MgCl_2$ for 15 min at 37°C to remove residual DNA. To concentrate the lentiviral vector batch, the supernatants were ultracentrifuged at 27,100 rpm for 90 min. After ultracentrifugation, pellets were resuspended in 50 to 100 ml of PBS overnight. The resuspended virus was finally processed through a series of short centrifugations (30 s at 13,500 rpm) to clarify the lentiviral solution of remaining debris. The batches of lentiviral particles were titrated by qRT-PCR using a SYBRÒ technology–based kit from Clontech/Takara and then stocked at −80°C until use for transduction. Lentivirus infection of human hepatocytes was done ex vivo before engraftment, at a multiplicity of infection of 5×10^4 or 1×10^5 VG per cell. Cells were infected for 30 min in suspension immediately upon thawing cryopreserved cells, were washed with PBS, and were prepared for engraftment as above.

Antibody dosing

The human-specific cMET antibody (Regeneron, REGN6753) was dosed one time per week at 25 mg/kg. The anti-CSF1R antibody (Regeneron, H4H32090P) was given two times per week at a concentration of 20 mg/kg. An anti–Fel d1 antibody (Regeneron, REGN1945), which does not bind any human or mouse proteins, was used as the control. Antibodies were diluted in PBS and given by intraperitoneal injection. Mice were randomized on the basis of hCD45 levels in the blood before anti-CSF1R or anti–Fel d1 treatment.

TaqMan real-time PCR

TaqMan real-time PCR was performed as previously described with slight modifications (*43*). Tissues were homogenized in RNAlater and were purified using the MagMAX-96 for microarrays total RNA isolation kit (Ambion by Life Technologies). Genomic DNA was removed using a ribonuclease-free DNase set (QIAGEN). mRNA was reverse-transcribed into cDNA using the SuperScript VILO master mix (Invitrogen Life Technologies) and a Veriti 96-well PCR thermal cycler (Thermo Fisher Scientific). cDNA was amplified with SensiFAST Probe Hi-ROX (Meridian Life Science) using 12k Flex System (Applied Biosystems). PCR reactions were done in triplicate, and *GAPDH* was used to normalize cDNA input differences. Data are reported as relative quantification using ΔΔCt. Primer and probe sequences are listed in table S1.

Supplementary Materials

This PDF file includes:

Figs. S1 to S8
Table S1

View/request a protocol for this paper from *Bio-protocol*.

REFERENCES AND NOTES

1. M. Grompe, S. Strom, Mice with human livers. *Gastroenterology* **145**, 1209–1214 (2013).
2. G. Sugahara, Y. Ishida, J. Sun, C. Tateno, T. Saito, Art of making artificial liver: Depicting human liver biology and diseases in mice. *Semin. Liver Dis.* **40**, 189–212 (2020).
3. H. Azuma, N. Paulk, A. Ranade, C. Dorrell, M. Al-Dhalimy, E. Ellis, S. Strom, M. A. Kay, M. Finegold, M. Grompe, Robust expansion of human hepatocytes in *Fah*$^{-/-}$/*Rag2*$^{-/-}$/*Il2rg*$^{-/-}$ mice. *Nat. Biotechnol.* **25**, 903–910 (2007).
4. M. Hasegawa, K. Kawai, T. Mitsui, K. Taniguchi, M. Monnai, M. Wakui, M. Ito, M. Suematsu, G. Peltz, M. Nakamura, H. Suemizu, The reconstituted 'humanized liver' in TK-NOG mice is mature and functional. *Biochem. Biophys. Res. Commun.* **405**, 405–410 (2011).
5. L. Zhang et al., Survival-assured liver injury preconditioning (SALIC) enables robust expansion of human hepatocytes in *Fah*$^{-/-}$ *Rag2*$^{-/-}$ *IL2rg*$^{-/-}$ rats. *Adv. Sci.* **8**, e2101188 (2021).
6. M. Carbonaro, J. Lee, E. Pefanis, M. Desclaux, K. Wang, A. Pennington, H. Huang, A. Mujica, J. Rojas, R. Ally, D. Kennedy, M. Brown, V. Rogulin, S. Moller-Tank, L. Sabin, B. Zambrowicz, G. Thurston, Z. Li, Efficient engraftment and viral transduction of human hepatocytes in an FRG rat liver humanization model. *Sci. Rep.* **12**, 14079 (2022).
7. C. Tateno, M. Kataoka, R. Utoh, A. Tachibana, T. Itamoto, T. Asahara, F. Miya, T. Tsunoda, K. Yoshizato, Growth hormone-dependent pathogenesis of human hepatic steatosis in a novel mouse model bearing a human hepatocyte-repopulated liver. *Endocrinology* **152**, 1479–1491 (2011).
8. E. Scorletti, R. M. Carr, A new perspective on NAFLD: Focusing on lipid droplets. *J. Hepatol.* **76**, 934–945 (2022).
9. M. Asrih, F. R. Jornayvaz, Inflammation as a potential link between nonalcoholic fatty liver disease and insulin resistance. *J. Endocrinol.* **218**, R25–R36 (2013).
10. V. Braunersreuther, G. L. Viviani, F. Mach, F. Montecucco, Role of cytokines and chemokines in non-alcoholic fatty liver disease. *World J. Gastroenterol.* **18**, 727–735 (2012).
11. D. Schmidt-Arras, S. Rose-John, IL-6 pathway in the liver: From physiopathology to therapy. *J. Hepatol.* **64**, 1403–1415 (2016).
12. K. Yamaguchi, Y. Itoh, C. Yokomizo, T. Nishimura, T. Niimi, H. Fujii, T. Okanoue, T. Yoshikawa, Blockade of interleukin-6 signaling enhances hepatic steatosis but improves liver injury in methionine choline-deficient diet-fed mice. *Lab. Invest.* **90**, 1169–1178 (2010).
13. J. Park, Y. Zhao, F. Zhang, S. Zhang, A. C. Kwong, Y. Zhang, H. H. Hoffmann, L. Bushweller, X. Wu, A. W. Ashbrook, B. Stefanovic, S. Chen, A. D. Branch, C. E. Mason, J. U. Jung, C. M. Rice, X. Wu, IL-6/STAT3 axis dictates the PNPLA3-mediated susceptibility to non-alcoholic fatty liver disease. *J. Hepatol.* **78**, 45–56 (2023).
14. C. Fang, X. Cai, S. Hayashi, S. Hao, H. Sakiyama, X. Wang, Q. Yang, S. Akira, S. Nishiguchi, N. Fujiwara, H. Tsutsui, J. Sheng, Caffeine-stimulated muscle IL-6 mediates alleviation of non-alcoholic fatty liver disease. *Biochim. Biophys. Acta Mol. Cell. Biol. Lipids* **1864**, 271–280 (2019).
15. L. Carulli, I. Canedi, S. Rondinella, S. Lombardini, D. Ganazzi, S. Fargion, M. de Palma, A. Lonardo, M. Ricchi, M. Bertolotti, N. Carulli, P. Loria, Genetic polymorphisms in non-alcoholic fatty liver disease: Interleukin-6-174G/C polymorphism is associated with non-alcoholic steatohepatitis. *Dig. Liver Dis.* **41**, 823–828 (2009).
16. S. Li, L. Chen, G. Lv, Interleukin-6 receptor blockade can increase the risk of nonalcoholic fatty liver disease: Indications from mendelian randomization. *Front. Pharmacol.* **13**, 905936 (2022).
17. Y. Ma, M. Gao, H. Sun, D. Liu, Interleukin-6 gene transfer reverses body weight gain and fatty liver in obese mice. *Biochim. Biophys. Acta* **1852**, 1001–1011 (2015).
18. E. Mas, M. Danjoux, V. Garcia, S. Carpentier, B. Ségui, T. Levade, IL-6 deficiency attenuates murine diet-induced non-alcoholic steatohepatitis. *PLOS ONE* **4**, e7929 (2009).
19. F. Hong, S. Radaeva, H. N. Pan, Z. Tian, R. Veech, B. Gao, Interleukin 6 alleviates hepatic steatosis and ischemia/reperfusion injury in mice with fatty liver disease. *Hepatology* **40**, 933–941 (2004).

20. S. Rebouissou, M. Amessou, G. Couchy, K. Poussin, S. Imbeaud, C. Pilati, T. Izard, C. Balabaud, P. Bioulac-Sage, J. Zucman-Rossi, Frequent in-frame somatic deletions activate gp130 in inflammatory hepatocellular tumours. *Nature* **457**, 200–204 (2009).
21. N. J. Hess, M. E. Brown, C. M. Capitini, G. V. H. D. Pathogenesis, GVHD pathogenesis, prevention and treatment: Lessons from humanized mouse transplant models. *Front. Immunol.* **12**, 723544 (2021).
22. M. Fujiyoshi, M. Ozaki, Molecular mechanisms of liver regeneration and protection for treatment of liver dysfunction and diseases. *J. Hepatobiliary Pancreat. Sci.* **18**, 13–22 (2011).
23. W. E. Naugler, B. D. Tarlow, L. M. Fedorov, M. Taylor, C. Pelz, B. Li, J. Darnell, M. Grompe, Fibroblast growth factor signaling controls liver size in mice with humanized livers. *Gastroenterology* **149**, 728–740.e15 (2015).
24. M. Jeffers, S. Rong, G. F. Vande Woude, Hepatocyte growth factor/scatter factor-Met signaling in tumorigenicity and invasion/metastasis. *J. Mol. Med. (Berl)* **74**, 505–513 (1996).
25. E. Houben, N. Hellings, B. Broux, Oncostatin M, an underestimated player in the central nervous system. *Front. Immunol.* **10**, 1165 (2019).
26. M. Ehlers, J. Grötzinger, F. D. deHon, J. Müllberg, J. P. Brakenhoff, J. Liu, A. Wollmer, S. Rose-John, Identification of two novel regions of human IL-6 responsible for receptor binding and signal transduction. *J. Immunol.* **153**, 1744–1753 (1994).
27. J. Bravo, J. K. Heath, Receptor recognition by gp130 cytokines. *EMBO J.* **19**, 2399–2411 (2000).
28. C. Ju, F. Tacke, Hepatic macrophages in homeostasis and liver diseases: From pathogenesis to novel therapeutic strategies. *Cell. Mol. Immunol.* **13**, 316–327 (2016).
29. G. Kolios, V. Valatas, E. Kouroumalis, Role of Kupffer cells in the pathogenesis of liver disease. *World J. Gastroenterol.* **12**, 7413–7420 (2006).
30. A. Sehgal, K. M. Irvine, D. A. Hume, Functions of macrophage colony-stimulating factor (CSF1) in development, homeostasis, and tissue repair. *Semin. Immunol.* **54**, 101509 (2021).
31. L. S. Feder, J. A. Todaro, D. L. Laskin, Characterization of interleukin-1 and interleukin-6 production by hepatic endothelial cells and macrophages. *J. Leukoc. Biol.* **53**, 126–132 (1993).
32. N. Lanthier, O. Molendi-Coste, P. D. Cani, N. Rooijen, Y. Horsmans, I. A. Leclercq, Kupffer cell depletion prevents but has no therapeutic effect on metabolic and inflammatory changes induced by a high-fat diet. *FASEB J.* **25**, 4301–4311 (2011).
33. W. Huang, A. Metlakunta, N. Dedousis, P. Zhang, I. Sipula, J. J. Dube, D. K. Scott, R. M. O'Doherty, Depletion of liver Kupffer cells prevents the development of diet-induced hepatic steatosis and insulin resistance. *Diabetes* **59**, 347–357 (2010).
34. L. Chen, H. Ye, X. Zhao, Q. Miao, Y. Li, R. Hu, Selective depletion of hepatic Kupffer cells significantly alleviated hepatosteatosis and intrahepatic inflammation induced by high fat diet. *Hepatogastroenterology* **59**, 1208–1212 (2012).
35. C. A. Norris, M. He, L.-I. Kang, M. Q. Ding, J. E. Radder, M. M. Haynes, Y. Yang, S. Paranjpe, W. C. Bowen, A. Orr, G. K. Michalopoulos, D. B. Stolz, W. M. Mars, Synthesis of IL-6 by hepatocytes is a normal response to common hepatic stimuli. *PLOS ONE* **9**, e96053 (2014).
36. T. Jostock, J. Müllberg, S. Özbek, R. Atreya, G. Blinn, N. Voltz, M. Fischer, M. F. Neurath, S. Rose-John, Soluble gp130 is the natural inhibitor of soluble interleukin-6 receptor transsignaling responses. *Eur. J. Biochem.* **268**, 160–167 (2001).
37. M. D. Giraldez, D. Carneros, C. Garbers, S. Rose-John, M. Bustos, New insights into IL-6 family cytokines in metabolism, hepatology and gastroenterology. *Nat. Rev. Gastroenterol. Hepatol.* **18**, 787–803 (2021).
38. S. Kang, T. Tanaka, M. Narazaki, T. Kishimoto, Targeting interleukin-6 signaling in clinic. *Immunity* **50**, 1007–1023 (2019).
39. K. Nakashima, M. Narazaki, T. Taga, Overlapping and distinct signals through leptin receptor (OB-R) and a closely related cytokine signal transducer, gp130. *FEBS Lett.* **401**, 49–52 (1997).
40. B. Akinci, A. Subauste, N. Ajluni, N. H. Esfandiari, R. Meral, A. H. Neidert, A. Eraslan, R. Hench, D. Rus, B. McKenna, H. K. Hussain, T. L. Chenevert, M. K. Tayeh, A. R. Rupani, J. W. Innis, C. S. Mantzoros, H. S. Conjeevaram, C. L. Burant, E. A. Oral, Metreleptin therapy for non-alcoholic steatohepatitis: Open-label therapy interventions in two different clinical settings. *Med. (N Y)* **2**, 814–835 (2021).
41. D. M. Valenzuela, A. J. Murphy, D. Frendewey, N. W. Gale, A. N. Economides, W. Auerbach, W. T. Poueymirou, N. C. Adams, J. Rojas, J. Yasenchak, R. Chernomorsky, M. Boucher, A. L. Elsasser, L. Esau, J. Zheng, J. A. Griffiths, X. Wang, H. Su, Y. Xue, M. G. Dominguez, I. Noguera, R. Torres, L. E. Macdonald, A. F. Stewart, T. M. DeChiara, G. D. Yancopoulos, High-throughput engineering of the mouse genome coupled with high-resolution expression analysis. *Nat. Biotechnol.* **21**, 652–659 (2003).
42. T. M. Dechiara, W. T. Poueymirou, W. Auerbach, D. Frendewey, G. D. Yancopoulos, D. M. Valenzuela, VelociMouse: Fully ES cell-derived F0-generation mice obtained from the injection of ES cells into eight-cell-stage embryos. *Methods Mol. Biol.* **530**, 311–324 (2009).
43. C. M. Williams, J. H. Calderon, E. Hock, Y. Jimenez, K. Barringer, M. Carbonaro, M. D. P. Molina-Portela, G. Thurston, Z. Li, C. Daly, Monomeric/dimeric forms of Fgf15/FGF19 show differential activity in hepatocyte proliferation and metabolic function. *FASEB J.* **35**, e21286 (2021).

Acknowledgments

Funding: All research activities described in this manuscript were funded by Regeneron Pharmaceuticals Inc., Tarrytown, NY, USA. **Author contributions:** Conceptualization and designing: M.C., G.T., and Z.L. Experiment design and data analysis: M.C., D.F., M.D., S.M.-T., and J.A. Experiment execution: K.W., H.H., A.Pa., A.Pe., J.Z., and G.P. Writing—original draft: M.C., G.T., and Z.L. Writing—review, critical scientific input, and editing: M.C., J.G., S.J., B.Z., A.M., J.C.L., C.D., M.S., J.A., G.T., and Z.L. Supervision: W.P., C.K., B.Z., A.M., J.C.L., L.E.M., C.D., M.S., G.T., and Z.L. **Competing interests:** A.Pe. was an employee of Regeneron Pharmaceuticals Inc. during the study until June 2022 and is currently employed by Pyxant Labs Inc. All other authors are current employees and stockholders of Regeneron Pharmaceuticals Inc. W.P., C.K., B.Z., A.M., J.C.L., L.E.M., and M.S. are current officers of Regeneron Pharmaceuticals Inc. M.C., A.M., G.T., and Z.L. are listed as inventors on a provisional patent application related to the work described in the manuscript. We confirm that there has been no significant financial support for this work that could have influenced its outcome. The authors declare that they have no other competing interests. **Data and materials availability:** All data needed to evaluate the conclusions in the paper are present in the paper and/or the Supplementary Materials. Proprietary animal models and antibodies may be made available from Regeneron Pharmaceuticals Inc. pending scientific review and a completed material transfer agreement. Requests for the animals or other reagents should be submitted to the corresponding author.

Submitted 4 November 2022
Accepted 9 March 2023
Published 14 April 2023
10.1126/sciadv.adf4490